HAL
open science

Micro- and nanocrystals of the iron(iii) spin-transition material [FeIII(3-MeO-SalEen)2]PF6

Antoine Tissot, Lionel Rechignat, Azzedine Bousseksou, Marie-Laure Boillot

To cite this version:

Antoine Tissot, Lionel Rechignat, Azzedine Bousseksou, Marie-Laure Boillot. Micro- and nanocrystals of the iron(iii) spin-transition material [FeIII(3-MeO-SalEen)2]PF6. Journal of Materials Chemistry, 2012, 22 (8), pp.3411. 10.1039/c2jm14913c . hal-03325399

HAL Id: hal-03325399

https://hal.science/hal-03325399

Submitted on 24 Aug 2021

HAL is a multi-disciplinary open access archive for the deposit and dissemination of scientific research documents, whether they are published or not. The documents may come from teaching and research institutions in France or abroad, or from public or private research centers.

L'archive ouverte pluridisciplinaire **HAL**, est destinée au dépôt et à la diffusion de documents scientifiques de niveau recherche, publiés ou non, émanant des établissements d'enseignement et de recherche français ou étrangers, des laboratoires publics ou privés.

Micro- and nanocrystals of the iron(III) spin-transition material $[Fe^{III}(3\text{-MeO-SalEen})_2]PF_6$.

Antoine Tissot,[a] Lionel Rechignat,[b] Azzedine Bousseksou,[b] Marie-Laure Boillot[*a]

Abstract

The elaboration of micro- and nanometric particles of $[Fe^{III}(3\text{-MeO-SalEen})_2]PF_6$ (H-3-MeO-SalEen being the condensation product of 3-methoxy-substituted salicylaldehyde and *N*-ethylethylenediamine), a spin-transition compound of molecular nature, is reported. A sudden precipitation approach, using butan-1-ol as an anti-solvent, has been shown to produce crystalline objects, whose size and shape can be modulated by varying the selected experimental parameters (temperature, solvent, polymeric confining agent). They are in the form of either needle-shaped (7500x640x215 (**a**); 3500x350x125 (**b**); 950x270 x35 nm^3 (**c**)) or spherical particles (18 ± 3 nm (**d**)). The chemical nature of these molecular materials has been confirmed by EDS and Raman spectroscopies. The RT powder X-ray diffractograms indicate the formation of size-reduced particles (**a-d**) of crystalline character, which correspond to the unperturbed phase previously reported by Hendrickson and coworkers. Magnetic, EPR and Raman investigations demonstrate the occurrence of a low-spin ↔ high-spin transition. In agreement with literature, disappearence of the weak hysteresis and decrease of cooperative character indicate weaker interactions within size-reduced particles. Two striking features: (i) the small shift in the transition temperatures from 162 K (bulk) to 153 K (18 nm) and (ii) the very quantitative spin transformation (fraction of HS residues ≤ 5%) contrast to those usually reported for coordination networks and point towards specificity of molecular nanomaterials.

1. Introduction

In the last decade, strategies for creating and mastering nanomaterials have considerably progressed and their unique functionalities[1] have been recognized for elaborating advanced materials exploited in several areas of technological applications. Recently, nanochemical methods adapted for switchable molecular-based materials, like spin-transition solids, have been investigated.[2] Spin-crossover solids show spectacular changes in their physical properties when their electronic spin states are switched between high-spin (HS) and low-spin (LS) states.[3] This electronic lability, which occurs under an external stimuli (T, P, hν, …), is intrinsically associated to the structural reorganization of the coordination core, i.e. changes of metal-ligand bond distances and bond angles.[4] The transformations proceed through electron-phonon coupling[5] and, as revealed by the course of equilibria and non-equilibria processes in materials, they are strongly impacted by cooperative long-range and short-range interactions, mainly of elastic nature.[3,6] Cooperative and hysteretic behaviors, characterized for a number of Fe^{II} molecular compounds, have attracted considerable attention due to their potential for applications[7] (displays, sensors, memories) and fundamental questions raised by the multiscale phenomenon (see [2] and references therein). Indeed, the cooperative processes at the macroscopic scale closely depend on the dimensionality (solid structuration), the strength (chemical, mechanical characteristics) and also the extension (size, crystalline quality of solid) of interactions. The bistability, which refers here to the occurrence for a system to be found in one of the two states existing for the same values of external parameters, may critically depend on the miniaturization of particles as well as on the characteristics of interfaces and particles surrounding. It is therefore essential to design methods allowing the nano-scale processing of spin-transition materials.

While a panel of techniques (co-precipitation, sol-gel processing, microemulsion, hydro- or solvothermal process, templated synthesis, biomimetic synthesis) has been experienced for robust materials (like metals or alloys, metal-oxides, chalconides, nitrides, halides, sulfides),[1] two types of approaches have been essentially exploited for molecule-based inorganic solids: growth of particles confined in nano- and microreactors or precipitation of particles in an anti-solvent.[8]

Concerning the spin-crossover materials,[2] the confinement of particle growth has been achieved either by microemulsion or sol-gel techniques, lithography-assisted deposition methods, leading to nanoparticles dispersion,[9,10,11] or nano-patterning, nanoscale organization,[12,13] respectively. Two families of relatively robust polymeric materials, stabilized by a 1D or 3D network of interconnected metal centers, have been selected. Fe^{II}-triazole and Fe^{II}(pyrazine)$[M(CN)_4]$ (M=Ni, Pd or Pt) compounds have successfully led to nano-sized objects by confining the syntheses within micelles (water-in-oil microemulsions technique), chitosan biopolymers[10] or pre-existent nanostructures.[12,13] With one exception,[9a] a first tendency associated to the size reduction of spin-transition nanoparticles, is a parallel between the decrease of the number of interacting centers and (i) the decrease in cooperativity and transition temperature (corresponding to a halfway-completed transition), (ii) an increase of HS residues. However, in view of literature,[9a,9c] the fact that behaviors of closely similar nanosized systems may vary, also suggests the influence of other parameters, such as the nature of chemical compound and the synthetic approach.

The technique of precipitation of nanoparticles in an anti-solvent has also been introduced. To the best of our knowledge, their applications to inorganic molecular materials[14] - for example the $[Mn_{12}O_{12}]$ cluster, a condensed species - are still very limited and this area remains almost unexplored. Because these materials are built up by discrete molecules organized via relatively weak supramolecular interactions, several parameters of synthesis may change the chemical compound himself (for example, through solvolysis, redox, acid-base reactions or deligandation) or modify its solid-state properties (via supramolecular

arrangement). Interestingly, a counterpart is the fact that, the coordination spheres of molecules located at nanoparticles interface should be identical to the core's ones. In addition, several molecular and supramolecular particularities (structural reorganization, thermo- or photochromism, temperature range, surrounding) can be tailored for investigations or applications of nanoparticles.

Recently, some of us have described the first elaboration of spin-crossover hybrid nanocomposites from a molecular prototype $[Fe^{II}(Mepy_3tren)](PF_6)_2$.[15] The spin-coating of a mixture of alkoxide precursors and Fe^{II} compound has led to the precipitation of Fe^{II} nanoparticles within the pores of silica thin films. It has been found that nanoparticles are well dispersed in transparent and easy-to-handle thin films; the observed sizes (between 750 and 50 nm) are controlled with relatively narrow size distributions. The sol-gel processing preserves the spin-crossover property of $[Fe^{II}(Mepy_3tren)](PF_6)_2$; the modifications of the thermal- and photo-induced characteristics are mainly related to the formation within silica of a new poorly crystalline polymorph. For this spin-crossover species, the effect of particles size is unresolved over the explored size range. All these features have led us to search for a combination of a molecular system and an approach allowing the synthesis of crystalline nanomaterials.

The nano-sized processing of Fe^{III} spin-crossover complexes has not yet been examined despite of attractive characteristics of their thermal- and photoswitching processes.[16] We report here the elaboration of nano- and microparticles of $[Fe^{III}(3\text{-MeO-SalEen})_2]PF_6$ by sudden precipitation. This ferric specimen exhibits a very cooperative spin transition at 162 K associated to a small thermal hysteresis.[17] The redox-stable compound belongs to a family of spin-crossover complexes, studied by D. N. Hendrickson and coworkers, who have reported how the first-order phase transition of $[Fe^{III}(3\text{-MeO-SalEen})_2]PF_6$ is perturbed by solid doping and grinding.[18] Recently, the mechanochemical properties of this sensitive compound have been examined and discussed on the basis of heat-capacity measurements.[19]

In the following, we present the syntheses and analyze the properties of $[Fe^{III}(3\text{-MeO-SalEen})_2]PF_6$ in the form of size-reduced particles. For comparison purpose, we examine also the powder XRD, Raman and EPR characterizations of the starting crystalline material.

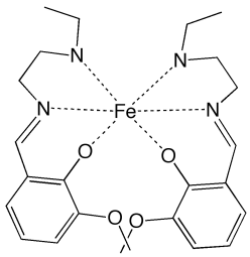

Scheme 1 Scheme of the cationic complex $[Fe^{III}(3\text{-MeO-SalEen})_2]^+$

2. Experimental

2.1 Syntheses

The molecular compound $[Fe(3\text{-MeO-SalEen})_2]PF_6$ was prepared as previously described in the literature.[17] Dark brown single crystals were obtained by slow evaporation of a methanolic solution of compound. Elemental Analysis: Formula $C_{26}H_{40}F_6FeN_4O_4P$ (%): Calcd: C 44.80, H 5.33, N 8.71; Found: C 44.76, H 5.29, N 8.71.

The syntheses of nano- and microparticles were achieved from the powdered material (or bulk) by sudden precipitation with an anti-solvent. Different experimental parameters were varied to control the average size of particles.

7.5 µm long microparticles synthesis (noted sample **a**): 10 mg of complex previously dissolved in 0.5 mL of acetonitrile were quickly added under vigorous stirring to 20 mL of butan-1-ol at 40°C. After 15 minutes, the microparticles were isolated by centrifugation and then, dispersed in 20 mL of a butan-1-ol solution containing 200 mg of PEG (polyethylene glycol, average MM = 6000 g/mol). The composite microparticles - polymer (**a**) was precipitated by cooling down the solution at 0 °C and then was isolated by centrifugation.

3.5 µm long microparticles (noted sample **b**) were synthetized by a similar procedure except that the precipitation step was carried out at 0 °C.

1 µm long microparticles (noted sample **c**) were synthetized by a similar procedure except that the compound (10 mg) was dissolved in 1 mL of acetone and the precipitation was carried out at -40°C. The compound was dissolved in acetone instead of acetonitrile for avoiding the freezing of solvent ($T_f^{acetone}$ = - 93.5 °C, $T_f^{acetonitrile}$ = - 45°C).

18 nm nanoparticles synthesis (noted sample **d**): 10 mg of the complex previously dissolved in 0.5 mL of acetonitrile were quickly added under vigorous stirring to a solution containing 200 mg of PEG, previously dissolved in 20 mL of butan-1-ol at 40°C. After 15 minutes, the solution was filtered with a 0.2 µm PTFE membrane and the composite nanoparticles - polymer **d** was precipitated by cooling down the solution at 0 °C and isolated by centrifugation.

In order to eliminate larger objects that could possibly be formed, the solution of nanoparticles was filtered (0.2 µm PTFE membrane) before the precipitation of polymer + nanoparticles composite.

2.2 Characterizations

The samples consisting in dispersions of particles (**a-d**) in PEG (5wt %), were characterized.

Powder X-ray diffraction diagrams were recorded at RT on a Philips Panalytical X'Pert Pro MPD powder diffractomer (Cu $K\alpha_1$, λ= 1.5405 Å) equipped with a fast detector. The measurements were performed over 1 hour (starting microcrystalline material or bulk) and one night (particles **a**-**d**), the powdered sample being deposited on a aluminium plate. The diffraction patterns were limited to the diffraction angles 2θ between 5 and 50 ° (microcrystalline powder) or 5 and 20 ° (particles dispersed in PEG).
Raman spectra were recorded using a Labram-HR (Jobin-Yvon) microspectrometer. The 632.8 nm line of a He-Ne laser (17 mW) was used as the excitation source and the heating effects of the sample were minimized by additional filters (OD = 2-3) on the excitation beam.
Magnetic measurements were carried out using a Quantum Design SQUID magnetometer (MPMS5S Model) calibrated against a standard palladium sample.
The X-Band EPR spectra were recorded at variable temperature with a Bruker ELEXSYS 500 spectrometer using an Oxford Instrument continuous-flow liquid nitrogen cryostat. The measurements were performed on the dispersion of particles **a**-**d**. Spectra were recorded between 0 and 7000 G with a microwave frequency of ca. 9.39 GHz; a microwave power of 2.0 mW; a modulation amplitude of 5 G; a modulation frequency of 100 kHz and a gain of 56 dB.

3. Results and discussion

3.1 Properties of the starting crystalline material

The powder X-ray diffraction pattern of the bulk sample of $[Fe^{III}(3\text{-MeO-SalEen})_2]PF_6$ was recorded at room temperature. The diffractogram (Fig. S1 in Electronic Supplementary Information) shows rather sharp and intense Bragg peaks. It corresponds as a whole to that previously reported for the unperturbed and high-spin sample of $[Fe^{III}(3\text{-MeO-SalEen})_2]PF_6$,[17] or that calculated from our variable temperature single-crystal X-ray investigation.[20] We note that the intense diffraction lines, observed at 9.5, 11.8 and 13.80 °, can be used for characterizing the size-reduced solids.
As previously described,[20] the magnetic data were collected for an assembly of small crystals of $[Fe^{III}(3\text{-MeO-SalEen})_2]PF_6$ at 0.5 K/min (Fig. S2, ESI). They characterize a complete and abrupt S=1/2 ↔ S=5/2 transition of ferric ions ($\chi_M T$ = 4.22 $cm^3.K.mol^{-1}$ at 300 K and 0.42 $cm^3.K.mol^{-1}$ at 10 K)‡. The spin transition occurs with a small hysteresis loop of 1.8 K ($T_{1/2}\uparrow$ = 163.2 K and $T_{1/2}\downarrow$ = 161.4 K), which compares to that reported for the unperturbed sample ($T_{1/2}$ = 162.31 K and $\Delta T_{1/2}$ = 2.8 K).[19]
Raman spectra of $[Fe^{III}(3\text{-MeO-SalEen})_2]PF_6$ were collected as a function of temperature between 350 and 100 K (see Fig. S3). Between 170 and 150 K, drastic changes in intensities/frequencies of vibrational modes suddenly appear in the spectra, due to the spin transition. Clear signatures of the thermal process are found in the low-frequency region. For example, different bands observed at high temperature (563, 598 and 626 cm^{-1}) vanish, while a band located at 621 cm^{-1} gains in intensity by lowering the temperature. They are thus assigned to HS and LS forms, respectively. In the high-energy range, the intense band assigned to C=N stretching vibrations also provides an unambiguous marker of the metal-ion spin-state switching (1599, 1615 and 1621 cm^{-1} in the HS phase versus 1603 cm^{-1} in the LS phase).
The Fe^{III} centers possessing an odd number of unpaired electrons, X-band EPR spectrometry can be used as a very sensitive technique to characterize the spin states of the materials and their interconversion. In the 100 K spectrum of the bulk, the pseudo-axial signal centered around g_e (g_1=2.22, g_2=2.19 and g_3=1.95) is identified as the one characterizing LS ions. The g values agree with those reported for the bulk (unperturbed Fe^{III} compound, g_1=2.220, g_2=2.187, g_3=1.946).[17]

3.2 Characterization of nano- and microcrystals: Morphology, Composition, Structure

The synthesis of particles was achieved by a method based on fast precipitation of compound without or with confinement of particles within PEG, a weakly coordinating polymer.
In absence of polymer, precipitations in the butan-1-ol anti-solvent led to the formation of needle-shaped microcrystals of $[Fe^{III}(3\text{-MeO-SalEen})_2]PF_6$ (see Fig. 1 a-c). Three sizes of microparticles (averaged at ca. 7.5 µm x 640 nm x 215 nm (**a**); 3.5 µm x 350 nm x 125 nm (**b**); 950 nm x 270 nm x 35 nm (**c**)) were obtained by fast precipitation at various temperatures. In these experiments, the precipitation itself was carried out in butan-1-ol. After centrifugation, particles were dispersed in a butan-1-ol solution of PEG and then the composite solid incorporating well-dispersed microparticles was precipitated. Average sizes were measured with TEM and SEM (see the particles and sizes, distributions in Fig. 1). In Fig. S4, SEM measurements performed with the composite powder noted **c** suggest some interactions between polymeric chains and particles, as it clearly appears that the needle-shaped particles are coated with polymer. The analysis by EDS confirms the presence of Fe and P atoms in the **a**, **b** and **c** needle-shaped samples of $[Fe^{III}(3\text{-MeO-SalEen})_2]PF_6$.
To sum up, in absence of polymer only microparticles of this Fe^{III} compound have been precipitated whereas, by the same method, nanoparticles of $[Mn_{12}O_{12}]$ clusters were isolated by Maspoch et al.[14b] Therefore, even if nanoparticles of $[Fe^{III}(3\text{-MeO-SalEen})_2]PF_6$ initially germinate in solution, because of their fast precipitation, aggregation and ripening quickly take place to form microcrystals. Addition of polymers prior to precipitation is thus necessary to avoid aggregation and eventually recover very small objects.
Indeed, spherical nanoparticles (**d**, 18 ± 3 nm) were isolated after a fast addition of an acetonitrile solution of complex on a butan-1-ol solution containing PEG, the mixture being stirred during 15 minutes. The dissolution of polymer in butan-1-ol prior to any complex addition is a condition to achieve an effective confinement effect of polymer. It was checked that, during the

precipitation of polymers, the size of particles does not significantly change. That is, after dispersion in butan-1-ol, the precipitated in-polymer particles present the same characteristics as those observed before precipitation. In the following, nano- or micrometric objects have been investigated in the form of in-PEG dispersions (5 wt %).

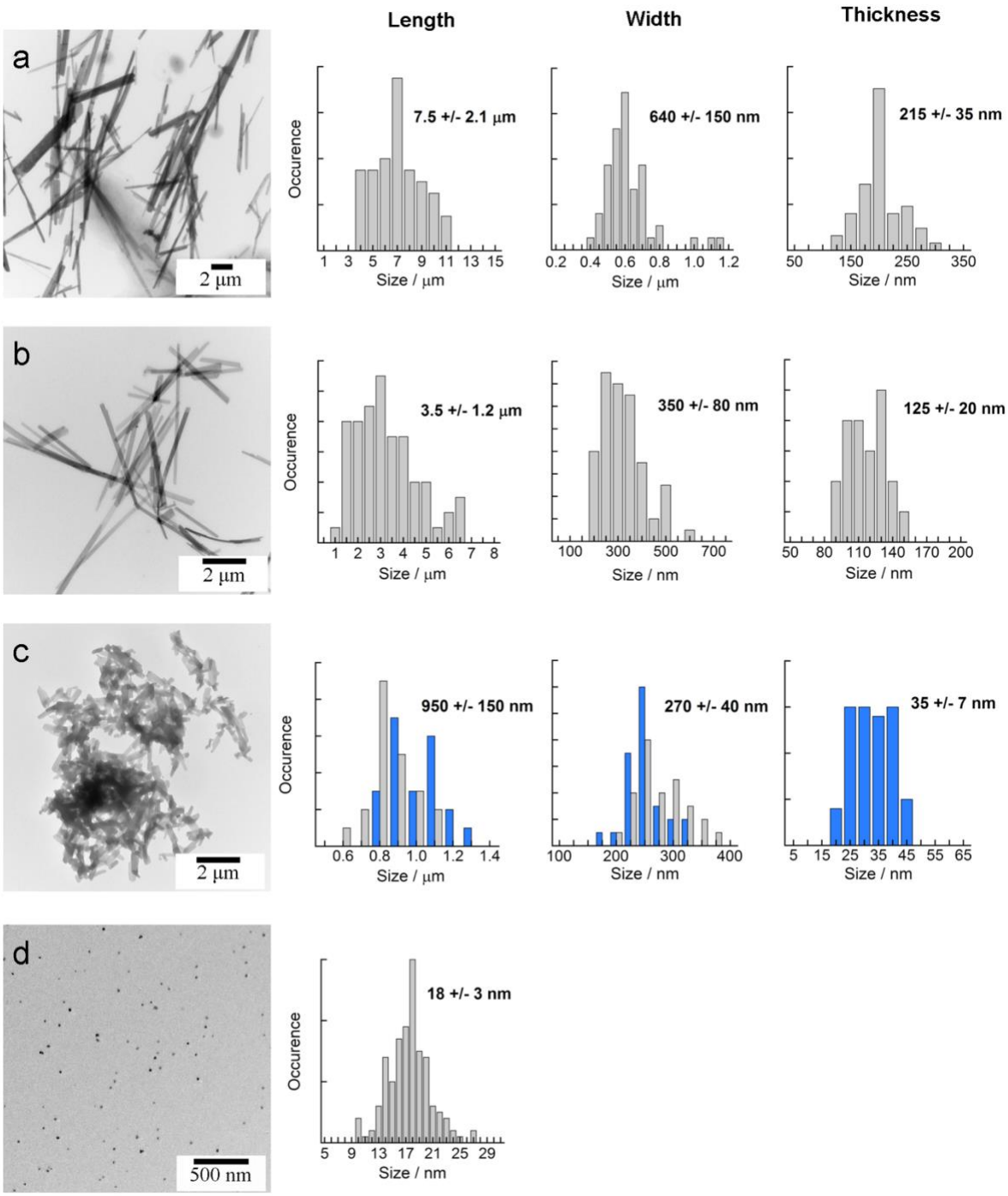

Fig. 1 $[Fe^{III}(3\text{-MeO-SalEen})_2]PF_6$ particles isolated with the preparations **a**, **b**, **c** and **d**: TEM images and corresponding size distribution curves determined by TEM (grey) and SEM (blue) measurements.

Additional characterization of the molecular material was provided by Raman measurements. This spectroscopic technique allows to carry out a selective analysis of the coordination compound despite the fact that the particles are embedded in polymers. Figure 2 shows the set of spectra of micro- and nanoparticles, as well as that of the starting material, collected at 250 K with a 532 nm excitation wavelength. From the spectra similarities and the detailed analysis of frequencies and intensities, we can firmly confirm the chemical integrity of molecules processed in the form of micro- and nano-particles. First indications on the spin-state of metal ions were also provided by the Raman data (Fig. 3 and S3). For all the samples, frequencies assigned to HS forms were detected at 250 and 170 K (for example at 563, 598 and 626 cm^{-1}). While the LS forms (peaks at 621 and

321 cm^{-1}) prevail in the 130 K spectrum of bulk and 7.5 μm particles (**a**), a mixture of LS and HS forms is observed for the smaller particle sizes (**b-d**) indicating a smooth spin transition and/or weak local heating effect due to the laser beam. At 100 K, no trace of HS species can be detected for the different composites (**a-d**). Therefore it is noticed that within the uncertainty of the measurements (ca. 5 %), an almost quantitative spin transformation occurs between 100 and 170 K for the micro- and nanosized particles.

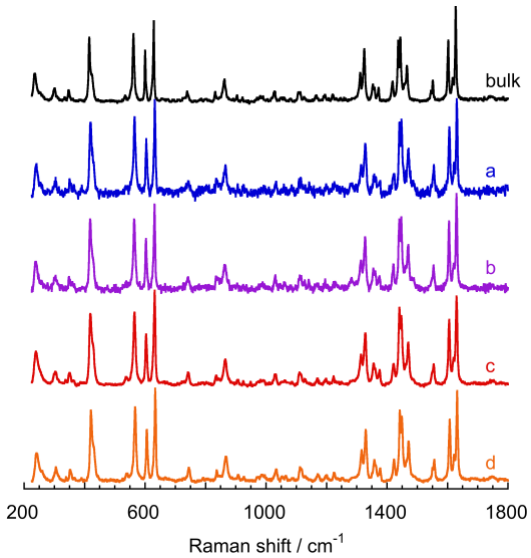

Fig. 2 Raman spectra of micro-, nanoparticles and the microcrystalline powder (bulk) of $Fe^{III}(3\text{-MeO-SalEen})_2]PF_6$ at 250 K. Labels **a-d** correspond to 7.5 (**a**); 3.5 (**b**); 1 (**c**) μm long microparticles or 18 nm nanoparticles (**d**).

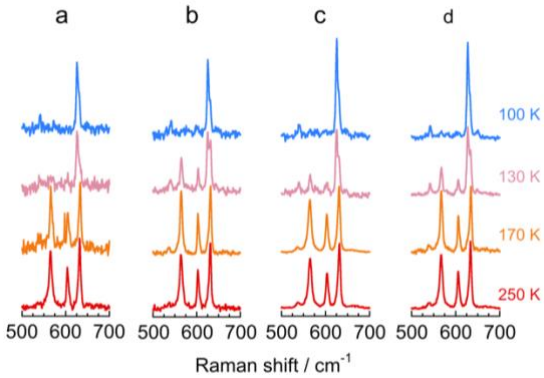

Fig. 3 Enlargement of the 500-700 cm^{-1} range of the Raman spectra of 7.5 (**a**), 3.5 (**b**), 1 (**c**) μm and 18 nm (**d**) particles showing the influence of a temperature decrease from 250 to 100 K.

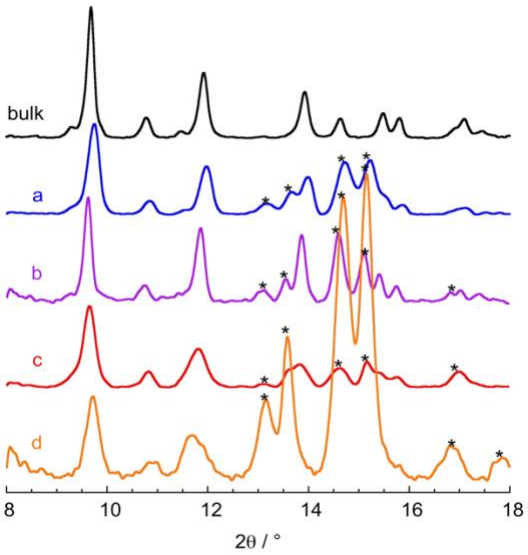

Fig. 4 Room temperature powder X-ray diffractograms of 7.5 (**a**), 3.5 (**b**), 1 (**c**) μm and 18 nm (**d**) composites compared to that of the microcrystalline starting material. The marked peaks (*) indicate the additional peaks due to the crystallinity of PEG.

The samples of $[Fe^{III}(3\text{-MeO-SalEen})_2]PF_6$ being isolated by sudden precipitation, one especially crucial point for the solid-state investigation concerns the nature of the spin-transition phase and its crystallinity. In Fig. 4, the room temperature X-ray diffractograms are plotted for 2θ values smaller than 18 ° since at larger values are observed signals due to crystalline PEG polymers. Several Bragg peaks previously characterized for the bulk sample are still present in the composites. Therefore the sudden precipitation process used for elaborating size-reduced objects preserves the crystalline character and the nature of the solid phase.

The width of diffraction lines can be related to the size of coherent domains. This analysis, based on the Scherrer equation, can not be done for microcrystals because of their shape anisotropy. However for the series of diffractograms, the progressive broadening of diffraction peaks, especially the one located at 11.9°, qualitatively shows a reduction of crystalline domain sizes. For the 18 nm spherical nanoparticles, the equation applied to the diffraction lines at 9.7° and 11.9°, provides crystalline domain sizes of ca. 26 and 16 nm, respectively. As these data are consistent with the TEM measurements, it can be infered that these particles **d** are very likely constituted by a crystalline single-domain.

The Raman and X-ray diffraction studies described above thus confirm the integrity of molecules and establish the nature and crystalline quality of the solid phase. At this stage, we can address the issue of the relationship, if any, between the size of particles and the thermal spin-state switching of the ferric compound. For this analysis, magnetic and EPR studies of micro- and nanocrystals are required.

3.3 Magnetic, EPR measurements of nano- and microcrystals

The temperature dependence of the magnetic properties of particles were measured at a scan rate of 1 $Kmin^{-1}$ between 10 and 250 K, the samples being in the form of an in-PEG dispersion for the purpose of avoiding any interactions or particles coalescence.[9e,11b]

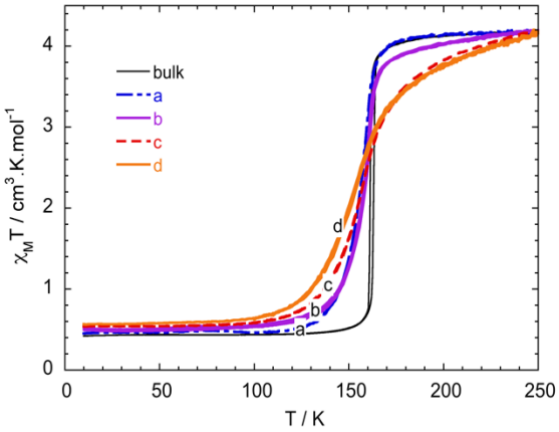

Fig. 5 Temperature dependence of $\chi_M T$ for in-PEG disoersion of nano- and microparticles (7.5 (**a**), 3.5 (**b**), 1 (**c**) μm and 18 nm (**d**) particles) of $Fe^{III}(3\text{-MeO-SalEen})_2]PF_6$. The data were collected at a 1 K/min scan rate between 10 and 250 K.

The $\chi_M T$ values can be extracted from magnetization data if we assume, as supported by our Raman measurements, that the HS fraction at 250 K is equal to 1. The treatment derives from the fact that the percentage of paramagnetic complexes within the composite formed with PEG is low (5 wt %) and not precisely known. As displayed in Fig. 5, the spin-transition curves vary with the samples. The very small hysteresis loop of 0.5 K, that is clearly noticable in the sample **a** curve, disappears for samples of lower sizes (**b-d**). By reducing the average size of crystallites, the transition temperatures slightly decrease from 162 K (bulk) to 153 K (**d**, 18 nm) and the transition curves are more progressive. The more pronounced assymmetry of transition curves, observed by decreasing the particles sizes, might be related to the size distribution effect,[21] even if these distributions can be considered as relatively limited (see in Fig. 1). In addition to assymmetry, we note that the **c** and **d** curves are especially close to each other, whereas the objects (size, shape) are very different. This point might be indicative that the thickness of needles (**c,** 35 nm) is a pertinent dimension for comparing the properties with spherical objects (**d**, 18 nm). Finally, the $\chi_M T$ limit at 10 K is almost unchanged as it varies between 0.42 $cm^3mol^{-1}K$ for the bulk corresponding to a LS Fe^{III} ion and 0.57 $cm^3mol^{-1}K$ for 18 nm (**d**) nanoparticles. We can infer from this observation the persistence of traces of HS residues, whose percentage can be estimated at ca. 5 % for the 18 nm nanoparticles.

X-band EPR measurements of micro- and nanoparticles were performed at variable temperature. In Fig. 6, the 100 K spectra of (**a-d**) samples show in the g~2 region the pseudo-axial S=1/2 signal previously characterized for the ferric complex.[17] An extremely weak evolution in the g_1 and g_2 components is observed that corresponds to subtle modulation of g and/or bandwidth values.

The samples (**a-d**) do not show any signals at g = 4.3 (impurities with S=5/2, E/D=1/3),[22] but in the low-field region a very weak and broad resonance centered around g = ca. 7.5 appears to be relatively more intense in the 100 K spectrum of 18 nm

particles (**d**). This signal, that gains in intensity at higher temperature, is ascribed to HS Fe^{III} ions, either in the form of HS residue or converted species. These observations are in a qualitative agreement with our magnetic investigation indicating a quasi complete spin conversion for (**a-c**) and a weak HS residue for (**d**).

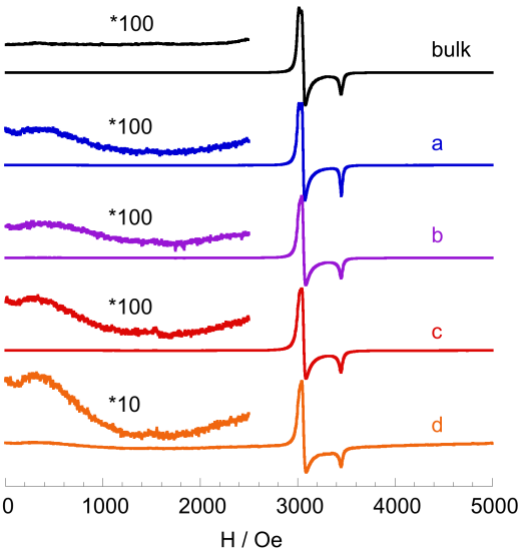

Fig. 6 100 K EPR spectra of $Fe^{III}(3\text{-MeO-SalEen})_2]PF_6$ in the form of composite powders **a-d** and comparison with the bulk.

Upon heating the sample **a** from 100 to 200 K (in Figure S4), the intensity of the LS signal decreases and concomitantly resonances due to HS species appear at g ~ 7.5 and ~ 2. The spin-state switching can be analyzed from the curves defined by the product of temperature and EPR absorption, the latter being the integrated EPR signal. Since this product varies as $\chi_M T$, the LS fraction (n_{LS} = 1-n_{HS}) is extracted from the area under this curve. Except a temperature shift (ca. 8 K) due to the temperature calibration, the transition curve derived from the variation of LS EPR signal shows a good correlation with the magnetic one. The spin-state switching process of sample (**a**) takes place over than 40 K.
Therefore, both EPR and Raman measurements only show the spectroscopic signatures of the studied Fe^{III} complex, here in the form of nano- and microcomposites. They demonstrate that the characteristics of molecular species (symmetry or distortion) are essentially preserved. In addition, this set of spectroscopic and magnetic data indicate very quantitative spin-transition processes occurring with changes in the cooperative character and transition temperature.

3.4 Discussion

The synthesis of molecule-based microcrystals was carried out in this work using a process allowing the formation of small nuclei by sudden precipitation. The temperature was used as a control parameter to tune the particles size between 7.5 (at 40 °C) and 1 µm (at -40 °C) long particles. As solubility decreases when the temperature is lowered, the amount of nuclei becomes higher at low temperature and hence particles are smaller. Moreover, the diffusion process in solution being slowed down at low temperature, it leads to the decrease of growth kinetics and thus to objects of smaller sizes. In contrast, the formation of 18 nm sized nanoparticles requires the dissolution of polymers in solution prior to any addition of metal complex, every other experimental parameters being kept identical with those of the microparticles **a** synthesis. This result indicates that the interaction between the polymer and the particles should be used for controling the kinetic of nanoparticles growth. The shape of the objects is spherical at lower size (**d**, 18 nm) while it is parallelepiped at larger sizes (**a-c**). A significant variation of the surface to volume ratio (**d**, 0.333 nm^{-1}; **c**, 0.067 nm^{-1}; **b**, 0.022 nm^{-1}; **a**, 0.013 nm^{-1} and $2x10^{-5}$ nm^{-1} for the bulk) is observed within the series.
Formation of crystalline nano-objects and preservation of the precursor phase, here a cooperative phase, are two features of major importance for the spin-transition property (see below). For these materials, changes in crystalline structure (polymorphism, desolvatation, amorphization) usually lead to drastic alteration of their spin-crossover characteristics or the transition disappearence (HS or LS stabilization). Different groups using the sudden precipitation approach have reported the formation of amorphous solids. Other works concerned nanosized samples of infinite coordination polymers[8] or $[Mn_{12}O_{12}]$ clusters.[14b] However nanocrystals of molecular materials were synthesized using an approach combining precipitation and confinement in SiO_2 matrices.[23] Applied to a spin-crossover type molecular material, this approach has led to an amorphous (or poorly crystallized) polymorph with new spin-crossover characteristics.[15] The loss of crystallinity and polymorphism were associated to the molecular nature and flexibility of this Fe^{II} complex. Organization of spin-crossover molecules and their packing, through relatively weak supramolecular interactions, may provide various lattices of comparable energies.[24] The fact that lattice and crystallinity of $[Fe^{III}(3\text{-MeO-SalEen})_2]PF_6$ were retained in the compound processed as nanoparticles can reasonably be related to the cooperative nature of the spin transition. Indeed, the first-order phase transition characterized for the bulk sample derives from the existence of strong elastic intersite interactions which are mediated by an extended 3D network

of supramolecular contacts.[20] The large lattice stabilization resulting from this organization can drive the formation of this phase, and thus preserve the solid-state properties, such as the thermal spin-state switching process.

The evolution of magnetic behaviors as a function of particles size shows interesting features. In the series studied in Fig. 5, the size reduction (and its distribution) is manifested by a decrease in transition temperature and cooperativity (for **a**-**d**), the quasi-immediate disappearence of hysteresis loop (for sample-sizes intermediate between **a** and **b**). This tendency, also shown by experimental works[9-11] and addressed theoretically,[2,21,25,26] is consistent with the fact that for a cooperative process completed over a shorter distance, a relative decrease of interactions strength and transition temperature may be expected for smaller objects. The similarity observed between the magnetic behaviors of **d** and **c** suggests that in case of needles-like objects, the size reduction effect is also related to the crystals thickness and particles shape, one point whose incidence is not yet well-known. One intriguing result is the observation of a quasi complete transition process, even for the 18 nm nanoparticles (ca. 5 % of residual HS species at low temperature). The frequent observation of a large increase of HS residues associated to the decrease of particles size,[9-11] raises the issue of what might be (i) the species remaining trapped in one spin state at any temperature, (ii) their chemical or physical origin. Different reasons can be considered from the background accumulated on spin-crossover materials,[2,3,17,18] although not necessarily specific to nanochemistry.

A first possibility is the formation of impurities with different magnetic properties. This is obviously related to the stability of metal complexes in the conditions (temperature, concentration, ionic strength, protic solvent, …) retained for synthesis and processing of nanoparticles. As shown above by the absence of new Raman or EPR signals (for example at g=4.3), this point is not critical for the iron(III) complex, isolated with a tridentate Schiff-Base, studied here. In contrast, a reduced stability can be anticipated, for example, for complexes sensitive to dioxygene and/or containing monodentate ligands .

A second possibility easily evoked concerns the presence at the nanoparticle surface of defects, i.e. coordination sites with different chemical environments (solvent as ligand or free-base function on polydentate ligand …) and consequently smaller ligand-field stabilizations than in bulk. Indeed, this type of defect is associated to the size reduction of coordination polymers, with a possible importance of dimensionality.[9a,9d,9e,11d] In the case of the ultra-small nanoparticles (3.8 nm) of $[Fe(pyrazine)\{(Ni(CN)_4)\}]$, a 3D coordination network isolated by some of the authors, 1/3 of spin-transition species were found to be associated to HS (1/3) and LS (1/3) residues while 60-70 % of iron atoms were localized at surface. The factors influencing the properties were the different environnements around metal ions at the surface combined to possible structural disorder, desolvatation. Note that for $[Fe^{III}(3\text{-MeO-SalEen})_2]PF_6$, the fraction of molecules localized at the particle pheriphery (1.1 nm layer) is equal to 32% (**d**), 7.3% (**c**), 2% (**b**) and 1.4% (**a**) (0.02% for bulk). The magnetic data, corroborated by the Raman and EPR ones are consistent with a fraction of HS residues (ca. 5 % for 18 nm nanocrystals, less for microcrystals) that is too low to derive from surface defects. This result, as the one in reference 15, confirms that HS or LS residues of molecular compounds are *a priori* not determined by chemical defects at surface.

A third origin of residual fractions, sometimes neglected despite indisputable evidences provided by studies of spin-crossover materials grinding or doping, is the possibility of ponctual defects or crystal imperfections favored by sudden precipitation or mechanical treatment. This influence is nicely exemplified by the study of the $[Fe^{III}(X\text{-SalEen})_2]Y$ series by Hendrickson and coworkers (see for example, the low-temperature shift by a sample doping with Cr(III) complexes).[17,18] Increasing the number of defects in bulk materials invariably leads to incomplete and progressive transition curves. This observation related to sample crystallinity and coherent domains was discussed in terms of nucleation and growth of phase transition.[17,18] Similar trends were observed for coordination polymers in the form of nanoparticles. For ca. 61x61x27 nm^3 objects of a 3D cyano-bridged iron network, Real et al[11a] have estimated a 14 % fraction of LS crystalline defects (core of nanoparticles) that should be compared to a 17 % fraction of HS surface defects. Another linked solid state characteristic, the dimension of coherent domains was analyzed by Létard et al with powder X-ray diffraction measurements.[9c] Except for the smallest nanoparticles (30 nm) of $Fe(NH_2\text{-trz})_3Br_2.3H_2O$ corresponding to a monodomain, the sizes of coherent domains were found to be much smaller than those of particles. The ratio of HS residue was related to the surface area of nanoparticles discarding the presence of crystalline imperfections. As mentioned above, the molecular spin-crossover materials are possibly subject to changes in crystalline structure (polymorphism,[24] desolvatation, …), with drastic consequences in their magnetic properties (formation of HS or LS phases). With respect to the micro- and nanoparticles of $[Fe^{III}(3\text{-MeO-SalEen})_2]PF_6$, the low level of HS residues can be accounted for, as mentioned above, to the formation of highly crystalline objects.

Beside the unwanted coalescence of particles, the interface -interaction between particles and surrounding, surfactants or polymers- may also affect the properties.[2,9e,9h] The effect of coating is thus a fourth factor sometimes envisaged in relation with chemical (hydrogen bond accepting groups[9e,9h]) or physical (viscosity,[9e,9h] matrice-mediated elastic vibrations,[11e] structural relaxation or 'chemical pressure'[11c]) properties. Today it is still difficult to evaluate their importance, their investigation is currently in progress.

Conclusions

The syntheses of the first micro- and nanoparticles of a molecular ferric spin-transition solid are reported here. It is demonstrated that the synthetic route - based on sudden precipitation and confinement in a polymer - preserves both the nature and the cristalline character of the solid-phase, while a molecular compound was selected. The formation of crystals of various size (from micro- to nanometric) and shape (needles and spheres) is shown to result from the choice of synthetic parameters and procedures. Only the smallest objects of ca. 18 nm of diameter have required the use of PEG for confining the particles growth and controlling their size distribution. It can be stressed, that this flexible synthetic approach opens interesting

potentialities (including technological applications) for spin-crossover materials of molecular nature, since these latter combine properties (bistability, cooperativity) to a variety of switchable characteristics (for ex. thermo-, piezo-, photochromism).[2,3,27] Within the series of micro- and nanocrystals studied here, we can conclude to a reduction of cooperative interactions with the particle size. We can also underline some specificities of molecular materials, such as the limited decrease of transition temperatures (< 6%), the very low content of HS residues and some possible influence of the particles shape.
The obtention of crystals at the frontier of micro- and nanometric structures is a key-feature for investigating photo-excitation mechanisms in the solid state, as more efficient, homogeneous and rapid transformations can be achieved in comparison to bulk materials (single-crystal or powders).[15,20] The dynamic of photoexcitation of these new materials is presently investigated by ultra-fast techniques and the relationship between the photoswitching process, the cooperativity and the size of objects is analyzed.

Acknowledgments

This work was supported by the CNRS, the French Ministery of research, ANR (ANR-09-BLAN-0212).
The authors warmly thank Drs. François Brisset, Daniele Jaillard (TEM and MEB measurements), Laurianne Billon (EPR measurements) and Pr. René Clément for their assistance. They also thank Florent Bridoux and Nerea Ruiz del Arbol Lasagabaster for their contribution in the syntheses.

Notes and references

[a] *ICMMO-ECI, UMR CNRS 8182, Univ. Paris-Sud 11, 91405 ORSAY, France. Fax: 33 16915 4754; Tel: 33 16915 4755; E-mail: marie-laure.boillot@u-psud.fr*
[b] *LCC, UPR CNRS 8241, Route de Narbonne, 31077 Toulouse cedex 04, France.*
† Electronic Supplementary Information (ESI) available: [RT Powder X-ray diffractogram of bulk and comparison with the calculated one; temperature dependence of the $\chi_M T$ product for the bulk; variable temperature Raman spectra of bulk and composites **a-d**; SEM images of composite **c**; variable temperature LS EPR signals of **a** and temperature dependence of HS fraction extracted from EPR data]. See DOI: 10.1039/b000000x/
‡ Footnotes. These values should be compared to $\chi_M T^{HS}$ = 4.375 $cm^3.K.mol^{-1}$ and $\chi_M T^{LS} \sim [g\sqrt{S(S+1)}]^2/8$ = 0.423 $cm^3.K.mol^{-1}$ with g^{EPR}=2.123 and S=1/2, for HS and LS species respectively.

1 (a) B. L. Cushing, V. L. Kolesnichenko and C. J. O'Connor, *Chem. Rev*., 2004, **104**, 3893; (b) C. N. R. Rao, S. R. C. Vivekchand, K. Biswas and A. Govindaraj, *Dalton Trans.* 2007, 3728.
2 A. Bousseksou, G. Molnar, L. Salmon and W. Nicolazzi, *Chem. Soc. Rev*., 2011, **40**, 3313.
3 O. Kahn, *Molecular Magnetism*, Wiley-VCH, New-York, 1993 ; Spin Crossover in transition Metal Compounds, I-III, *Top. Curr. Chem.*, P. Gütlich and H. A. Goodwin eds, Springer, Berlin, 2004, vol. **233-235**.
4 E. König, Prog. *Inorg. Chem*., 1987, **35**, 527. P. Guionneau, M. Marchivie, G. Bravic, J.-F. Létard and D. Chasseau, *Top. Curr. Chem*., eds P. Gütlich and H.A. Goodwin, Springer, Berlin, 2004, vol. **234**, p 97.
5 J. Nasser, *Eur. Phys. J. B* , 2001, **21**, 3.
6 H. Spiering, *Top. Curr. Chem*., eds P. Gütlich and H.A. Goodwin, Springer, Berlin, 2004, vol. **235**, p 171.
7 J.-F. Létard, P. Guionneau and L. Goux-Capes, *Top. Curr. Chem*., eds P. Gütlich and H.A. Goodwin, Springer, Berlin, 2004, vol. **235**, p 221.
8 A. M. Spokoyny, D. Kim, A. Sumrein and C. A. Mirkin, *Chem. Soc. Rev.*, 2009, **38**, 1218; A. Carné, C. Carbonell, I. Imaz and D. Maspoch, *Chem. Soc. Rev*., 2011, **40**, 291.
9 See for example: (a) E. Coronado, J. R. Galan-Mascaros, M. Monrabal-Capilla, J. Garcia-Martinez and P. Pardo-Ibanez, *Adv. Mater*., 2007, **19**, 1359; (b) T. Forestier, S. Mornet, N. Daro, T. Nishihara, S. Mouri, K. Tanaka, O. Fouche, E. Freysz and J.-F. Létard, *Chem. Commun*., 2008, 4327; (c) T. Forestier, A. Kaiba, S. Pechev, D. Denux, P. Guionneau, C. Etrillard, N. Daro, E. Freysz and J.-F. Létard, *Chem.-Eur. J*., 2009, **15**, 6122; (d) J. R. Galan-Mascaros, E. Coronado, A. Forment-Aliaga, M. Monrabal-Capilla, E. Pinilla-Cienfuegos and M. Ceolin, *Inorg. Chem*., 2010, **49**, 5706; (e) A. Tokarev, L. Salmon, Y. Guari, W. Nicolazzi, G. Molnar and A. Bousseksou, *Chem. Commun*., 2010, **46**, 8011; (f) L. Salmon, G. Molnar, D. Zitouni, C. Quintero, C. Bergaud, J.-C. Micheau and A. Bousseksou, *J. Mater. Chem.*, 2010, **20**, 5499; (g) C. Faulmann, J. Chahine, I. Malfant, D. de Caro, B. Cormary and L. Valade, *Dalton Trans*., 2011, **40**, 2480; (h) A. Tokarev, L. Salmon, Y. Guari, G. Molnar and A. Bousseksou, *New J. Chem*., DOI: 10.1039/c1nj20218a.
10 J. Larionova, L. Salmon, Y. Guari, A. Tokarev, K. Molvinger, G. Molnar and A. Bousseksou, *Angew. Chem. Int. Ed.*, 2008, **47**, 1.
11 See for example: (a) I. Boldog, A. B. Gaspar, V. Martinez, P. Pardo-Ibanez, V. Ksenofontov, A. Bhattacharjee, P. Gütlich and J. A. Real, *Angew. Chem. Int. Ed*., 2008, **47**, 6433; (b) F. Volatron, L. Catala, E. Rivière, A. Gloter, O. Stéphan and T. Mallah, *Inorg. Chem*., 2008, **47**, 6584; (c) V. Martinez, I. Boldog, A. B. Gaspar, V. Ksenofontov, A. Bhattacharjee, P. Gültich and J. A. Real, *Chem. Mater*., 2010, **22**, 4271; (d) C. Bartual-Murgui, N. A. Ortega-Villar, H. J. Shepherd, M. C. Munoz, L. Salmon, G. Molnar, A. Bousseksou and J.-A. Real, *J. Mater. Chem.*, 2011, **21**, 7217; (e) Y. Raza, F. Volatron, S. Moldovan, O. Ersen, V. Huc, C. Martini, F. Brisset, A. Gloter, O. Stephan, A. Bousseksou, L. Catala and T. Mallah, *Chem. Commun.*, DOI: 10.1039/c1cc14463d.
12 G. Molnar, S. Cobo, J. A. Real, F. Carcenac, E. Daran, C. Vieu and A. Bousseksou, *Adv. Mater*., 2007, **19**, 2163.
13 M. Cavallini, I. Bergenti, S. Milita, G. Ruani, I. Salitros, Z.-R. Qu, R. Chandrasekhar and M. Ruben, *Angew. Chem. Int. Ed*., 2008, **47**, 8596.
14 (a) C. A. Johnson, S. Sharma, B. Subramaniam and A. S. Borovik, *J. Am. Chem. Soc*., 2005, **127**, 9698; (b) I. Imaz, F. Luiz, C. Carbonera, D. Ruiz-Molina and D. Maspoch, *Chem. Commun*., 2008, 1202.
15 A. Tissot, J.-F. Bardeau, E. Rivière, F. Brisset and M.-L. Boillot, *Dalton Trans*., 2010, **39**, 7806.
16 M. Nihei, T. Shiga, Y. Maeda and H. Oshio, *Coord. Chem. Rev*., 2007, **251**, 2606; C. Brady, J. J. McGarvey, J. K. McCusker, H. Toftlund and D. N. Hendrickson, *Top. Curr. Chem*., eds P. Gütlich and H.A. Goodwin, Springer, Berlin, 2004, vol. **235**, p 1; M. Lorenc, J. Hebert, N. Moisan, E. Trzop, M. Servol, M. Buron-Le Cointe, H. Cailleau, M.-L. Boillot, E. Pontecorvo, M. Wulff, S. Koshihara and E. Collet, *Phys. Rev. Lett*., 2009, **103**, 028301.

[17] M. S. Haddad, M. W. Lynch, W. D. Federer and D. N. Hendrickson, *Inorg. Chem*., 1981, **20**, 123.
[18] M. S. Haddad, W. D. Federer, M. W. Lynch and D. N. Hendrickson, *Inorg. Chem*., 1981, **20**, 131.
[19] M. Sorai, R. Burriel, E. F. Westrum, Jr and D. N. Hendrickson, *J. Phys. Chem. B*, 2008, **112**, 4344.
[20] A. Tissot, R. Bertoni, L. Toupet, E. Collet and M.-L. Boillot, *J. Mater. Chem.*, DOI:10.1039/C1JM14163E.
[21] A. Muraoka, K. Boukheddaden, J. Linarès and F. Varret, *Phys. Rev. B*, 2011, **84**, 054119.
[22] A. J. Simaan, F. Banse, J.-J. Banse, K. Wieghardt and E. Bill, *Inorg. Chem.*, 2001, **40**, 6538.
[23] N. Sanz, A.-C. Gaillot, Y. Usson, P. L. Baldeck and A. Ibanez, *J. Mater. Chem*., 2000, **10**, 2723; B. Cormary, I. Malfant and L. Valade, *J. Sol-Gel Sci. Technol*., 2009, **52**, 19.
[24] See for example: J. - F. Létard, C. Chastanet, O. Nguyen, S. Marcén, M. Marchivie, P. Guionneau, D. Chasseau and P. Gütlich, *Monatsch. Chem.*, 2003, **134**, 165; G. S. Matouzenko, A. Bousseksou, S. Lecocq, P. J. Van Koningsbruggen, M. Perrin, O. Kahn and A. Collet, *Inorg. Chem*., 1997, **36**, 5869 ; C. F. Sheu, S. Pillet, Y. C. Lin, S. Chen, I. J. Hsu, C. Lecomte and Y. Wang, *Inorg. Chem*., 2008, **47**, 10866 ; A. Collet, M.-L. Boillot, J. Hebert, N. Moisan, M. Servol, M. Lorenc, L. Toupet, M. Buron-Le Cointe, A. Tissot and J. Sainton *Acta Cryst. B*, 2009, **65**, 474.
[25] T. Kawamoto and S. Abe, *Chem. Commun*., 2005, 3933.
[26] See for example: W. Nicolazzi, S. Pillet and C. Lecomte, *Phys. Rev. B*, 2008, **78**, 174401; C. Enachescu, L. Stoleriu, A. Stancu and A. Hauser, *Phys. Rev. Lett.*, 2009, **102**, 257204; C. Enachescu, M. Nishino, S. Miyashita, A. Hauser, A. Stancu and L. Stoleriu, *EPL*, 2010, **91**, 27003.
[27] M.-L. Boillot, S. Pillet, A. Tissot, E. Rivière, N. Claiser and C. Lecomte, *Inorg. Chem*., 2009, **48**, 4729.